On the effects of the Solar Wind Alfvénic Mach number on the Bow-Shock dynamics

E. Cazzola[i], D. Fontaine[i], P. Savoini[i], C. Moissard[i], T.Huret[i], M. Akhavan-Tafti[i+]

([i]) LPP - CNRS - École polytechnique - UPMC, ([+]) CLaSP - University of Michigan Ann Arbor

PRESENTED AT:

AGU FALL MEETING
Online Everywhere | 1–17 December 2020

SECTION 1) METHODOLOGY AND SIMULATION SETUP

We show here some results of a study campaign on the tridimensional effects of the Quasi-Perpendicular interaction between a steady Solar Wind flow at different Alfvénic Mach numbers and the terrestrial Bow-Shock by means of hybrid simulations.

The simulations were performed with the fully 3D multi-species MPI-parallel hybrid code LatHyS (Modolo et al. 2005)developed on the basis of the CAM-CL scheme (Matthews 1994) and already designed for the simulation of dynamic boundaryvalue problems, such as to study the dynamics of incoming Solar Wind or of transient extreme space weather phenomena – e.g. CIRs and CMEs (Turc et al. 2015). The code coordinate's system is Cartesian, featuring open boundary conditions at the inlet/outlet edges and periodic boundaries elsewhere.

All the results are shown in GSE coordinates, by neglecting the terrestrial geomagnetic inclination. The different incoming Solar Wind conditions are taken from the OMNI NASA database by selecting scenarios with an increasing Alfvénic Mach number, as summarized in Table I. For the purpose of this work, only the two cases charted in Table I will be considered. For sake of comparison we chose the same ions plasma $\beta = 0.4$ for both simulations.

Year-DOY	Ma	B [nT]	N [cm^{-3}]	V [$km.s^{-1}$]	ρV^2 [nPa]
2019-132	3.87	6.9	2.9	342	0.567
2019-244	9.50	6.2	3.4	697	2.763

Table I: The first column being the Day-of-Year DOY on which the Solar Wind data were observed, the second column the Alfvénic Mach number,columns three through five being the pristine, respectively, Interplanetary Magnetic Field, Solar Wind particle density and bulk Velocity. The last column indicates the incoming Solar Wind dynamic pressure.

We represent the obstacle as a magnetic dipole object rescaled to a value of 10 di, where di is the ion skin depth referred to the pristine SW conditions.

The Interplanetary Magnetic Field (IMF) direction is fixed to generate a Quasi-Perpendicular interaction for all the cases analyzed. Particularly, the IMF will be directed along the Y-axis, unless otherwise specified, with the angle between the Interplanetary Magnetic Field and the Bow-Shock nose $B_{n\Theta} = 90^{\circ}$. No regions on the BS surface do approach angles less than 45˚, so that the Quasi-Parallel dynamics can be excluded from this scenario. The situation is depicted in the side Figure, with the Solar Wind entering the system from the left boundary and flowing in a radial direction along X.
The following results have been validated with the Bow-Shock fitting model proposed in Jerab et al. 2005 obtaining a good agreement.

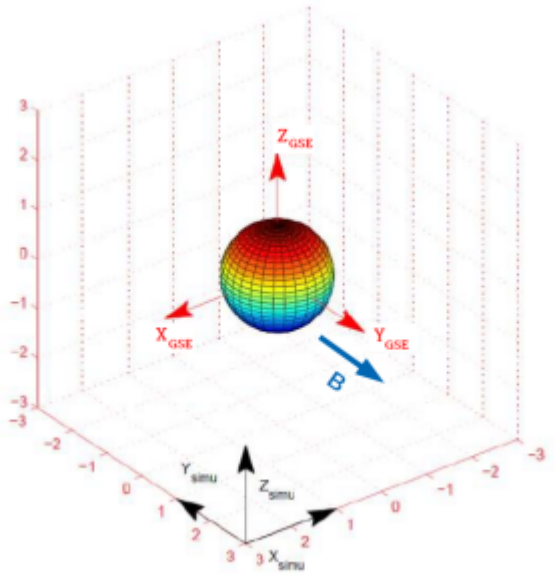

SECTION 2) ANALYZING THE GLOBAL SCALE RESULTS

In Figure 1 we show the global Bow-Shock (BS) response to the Solar Wind conditions summarized in Table I once the evolution has achieved the steady-state conditions. The situation on two half-planes are analyzed in term of the magnetic field intensity: on the ecliptic plane X-Y (upper panels) and the plane perpendicular to it (i.e. X-Z) at Y = 0 (lower panels). Only the Dawn sector at negative Ys and the northern hempishere at positive Zs are represented here thanks to the symmetric nature of the system.

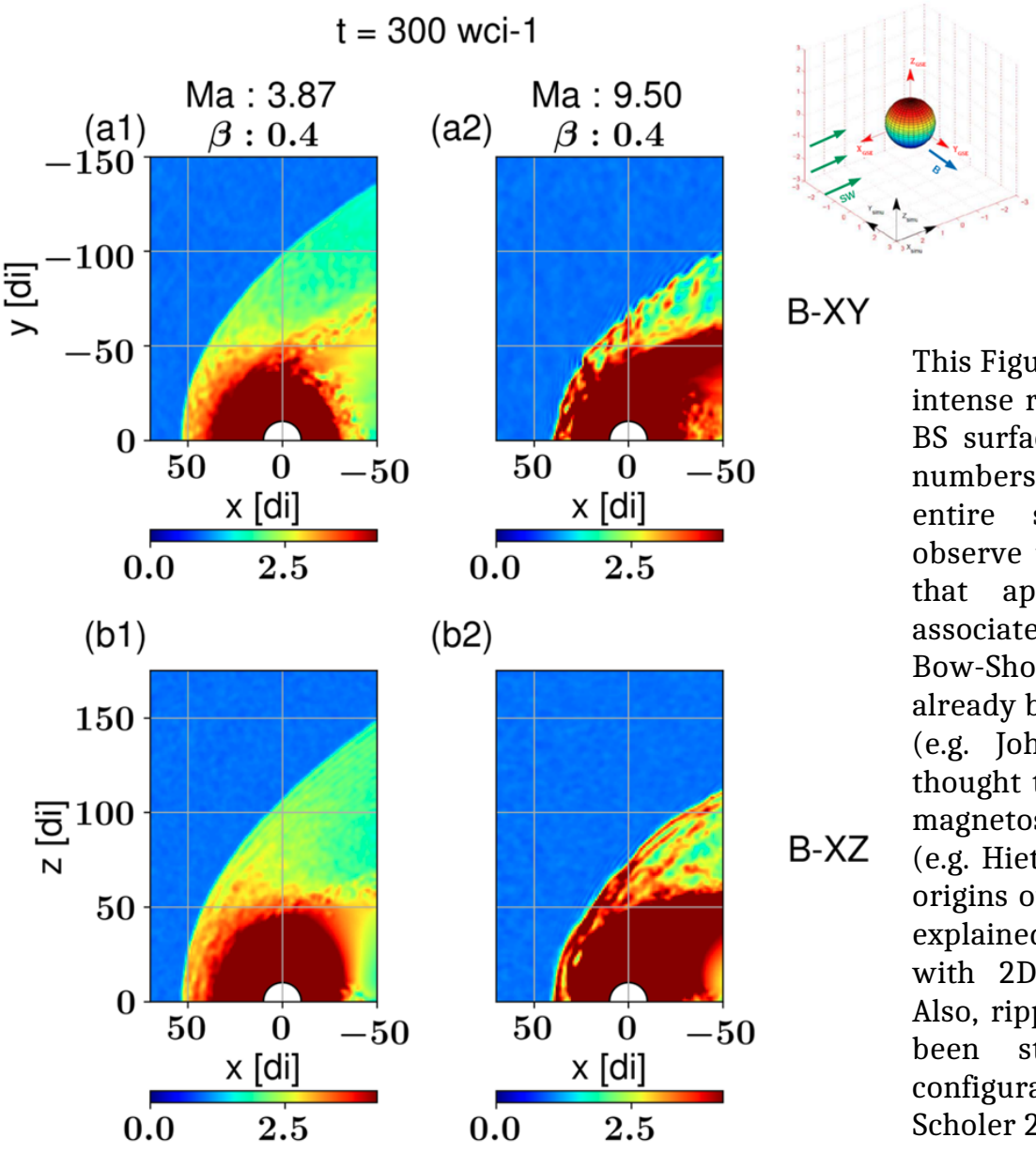

Fig. 1: Map of the magnetic field intensity on half of the ecliptic plane (X-Y) - upper panels - and the half-plane perpendicular to this latter (X-Z) -lower panels - for the two cases here considered with Ma = 3.87 and Ma = 9.50. Values are normalized to the IMF conditions. The IMF is composed of B_y only directed towards positive Y. Coordinates in GSE.

This Figure illustrates the onset of an intense rippling phenomenon on the BS surface for relatively high Mach numbers propagating along the entire surface. Additionally, we observe the onset of a set of waves that appears to be specifically associated to the ripples dynamics. Bow-Shock rippling phenomena have already been observed with satellites (e.g. Johlander et al. 2016) and thought to be the dynamic source of magnetosheath jets and plasmoids (e.g. Hietala & Plaschke 2013). The origins of these ripples were initially explained in Winske & Quest 1988 with 2D-planar shock simulations. Also, ripples on shock surfaces have been studied in more ad-hoc configurations (e.g. in Burgess & Scholer 2007).

On the other hand, Figure 1 also shows that the ripples are only observed on the ecliptic plane (X-Y), whereas on perpendicular plane X-Z only very low frequency oscillations are seen (lower panels).

We investigated whether the IMF direction may somehow influence the rippling behavior. We have switched the IMF direction from lying on to the X-Y plane to lying on to the X-Z plane, in this latter case directed both northwards and southwards. The pure Quasi-Perpendicularity is still respected, but particles are now gyrating perpendicularly to another plane. Figure 2 compares the three situations for the case with M_A = 9.50: the angle $B_{V\Theta}$ represents the Quasi-Perpendicular condition in terms of the angle between the directions of the IMF and the Solar Wind velocity, whereas ψ is the angle between the Z-direction and the X-Y plane. From these outcomes we can states that the ripples always develop mainly on the plane where the IMF lies, with the other perpendicular planes showing only an low frequency oscillation.

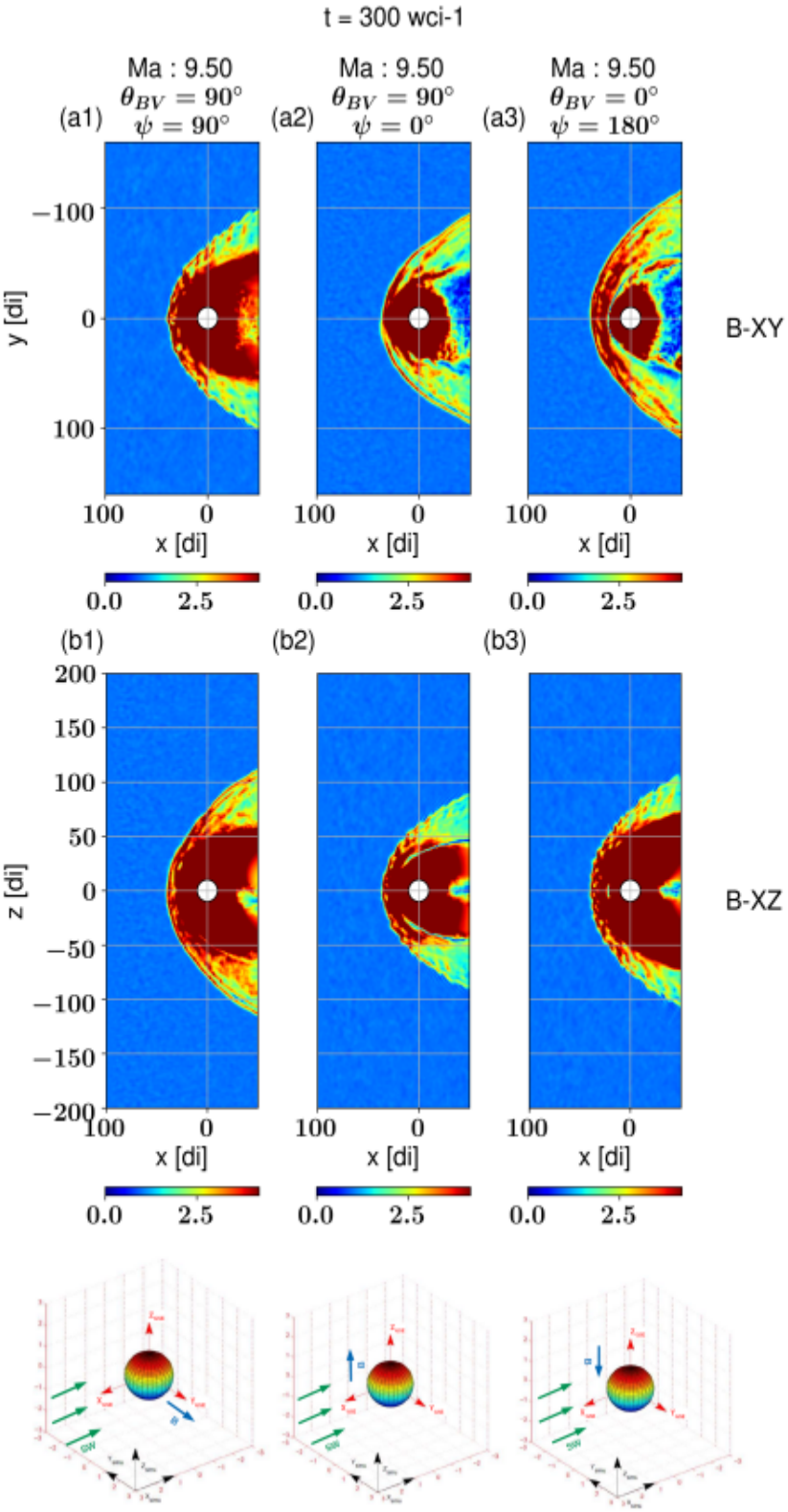

Fig. 2: Map of the magnetic field intensity for the specific scenario with M_A = 9.50 and different orientations of the IMF magnetic field with respect to the X-Z plane (ψ is the angle between the X-Y plane and the Z direction, whereas $B_{V\Theta}$ is the angle between the IMF and bulk SW velocity): panels (a1) and (b1)represent the reference case with IMF lying on the X-Y plane and directed towards +Y, panels (a2)-(b2) represent with the IMF lying on the X-Z plane and ψ=0 (directed +Z) and panels (a3)-(b3) the case with IMF lying on the X-Z plane and ψ=180 (directed -Z). Values are normalized to the pristine IMF intensity. Coordinates in GSE.

SECTION 3) CHARACTERIZING THE RIPPLES

In order to characterize better the ripples in terms of propagating direction and velocity, we addressed an analysis similar to that carried out in Burgess et al. 2007, only that, unlike their 2D planar case, here we have to deal with a curved tridimensional surface. To do so, we used the following technique (see Figure 3 as reference):

(i) We have identified the best quantity able to neatly highlight the Bow-Shock surface, such as the Z-component of the current density, which allows evidencing the shock wave front in detail - panel (a).

(ii) By exploiting the potentiality of computer simulations in providing structured grid outputs, for each Y-coordinate we screen out all the values along the X-coordinate until meeting a value grater than a specific threshold Jz/J > χ, χ being the pristine reference value (for case shown here χ = 0.27). Once found, that particular position (i.e. pixel) is flipped to 1, the screening is stopped and the following Y-coordinate is considered. As result, we obtained a profile like that shown in panel (b).

(iiI) At this point we can enter these coordinates into a linear regression method tool based on the following quadratic surface equation

$$x\,(y,z) = a_{2,0}y^2 + a_{1,1}yz + a_{0,2}z^2 + a_{1,0}y + a_{0,1}z + a_{0,0}$$

to obtain a result like the curve superimposed in panel (c) - and enlarged in panel (d) - which will now represent our nominal Bow-Shock surface.

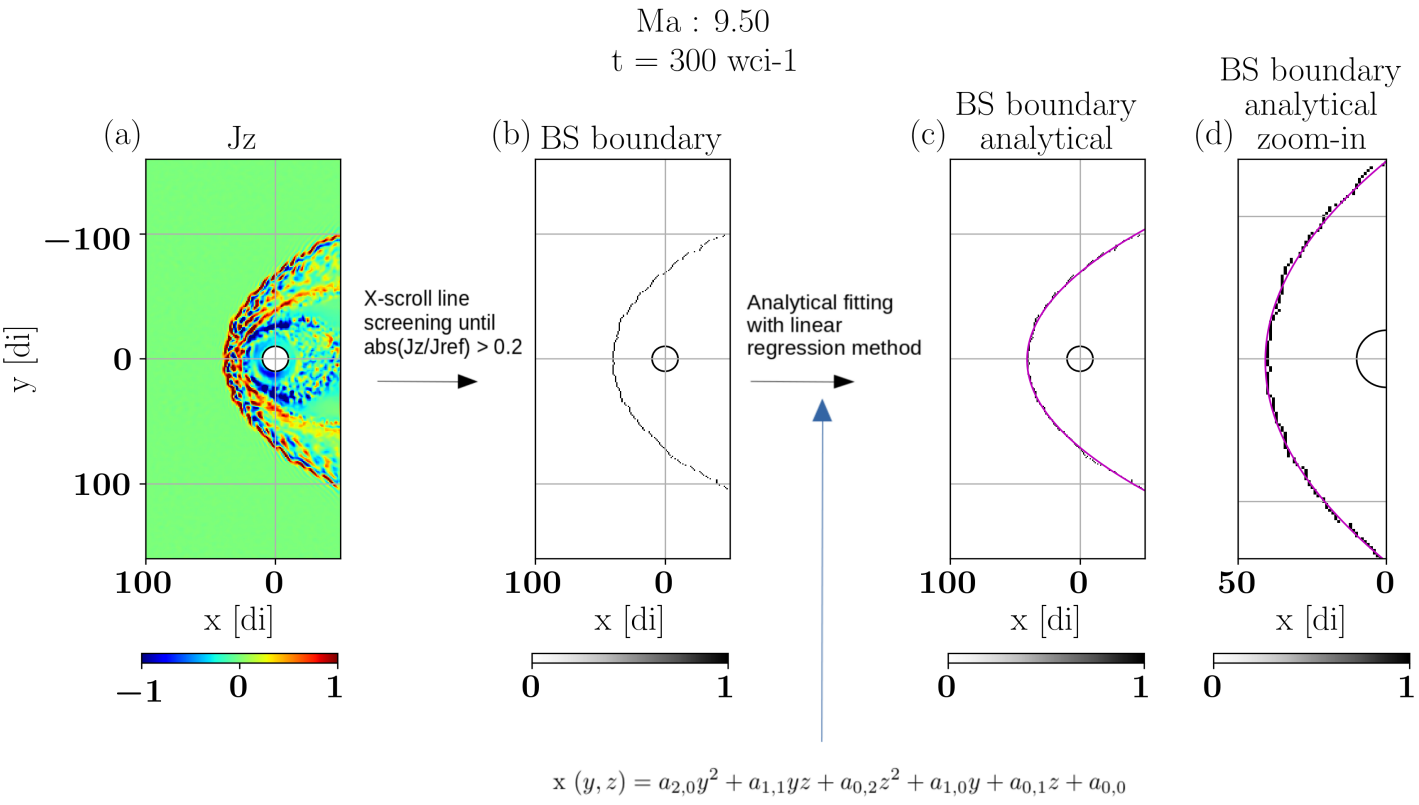

Fig. 3: Stepflow adopted to fit the Bow-Shock surface with an analytical nominal surface. Panel (a) represents a map of the current density in the Z direction. Panel (b) shows the outcome obtained upon applying the technique explained in the text, with χ = 0.27. Panel (c) plots the profile of panel (b) with the nominal surface superimposed as obtained by applying a linear regression method on the quadratic surface equation shows in the text.
Finally, panel (d) shows a zoom-in to highlight the surface-ripples crossing.

Upon determining the Bow-Shock nominal surface, we can use this information for different type of analyses, including an analysis of the ripples temporal evolution.
By plotting the magnetic field intensity at the position of the nominal surface for all the time steps, we obtain the outcome shown in Figure 4 (plotting-time resolution is 0.5 wci^{-1}).

Particularly, we have compared two specific situations at Ma = 9.50: panel (a1) shows the case with the IMF directed towards +Y and panel (a2) shows the case with a reversed IMF direction - Φ_{BX} represents the angle between the IMF direction and the X-coordinate in GSE system. This angle takes the value of +90˚ when $B = B_y e_y$,and the value -90˚ when $B = -B_y e_y$.

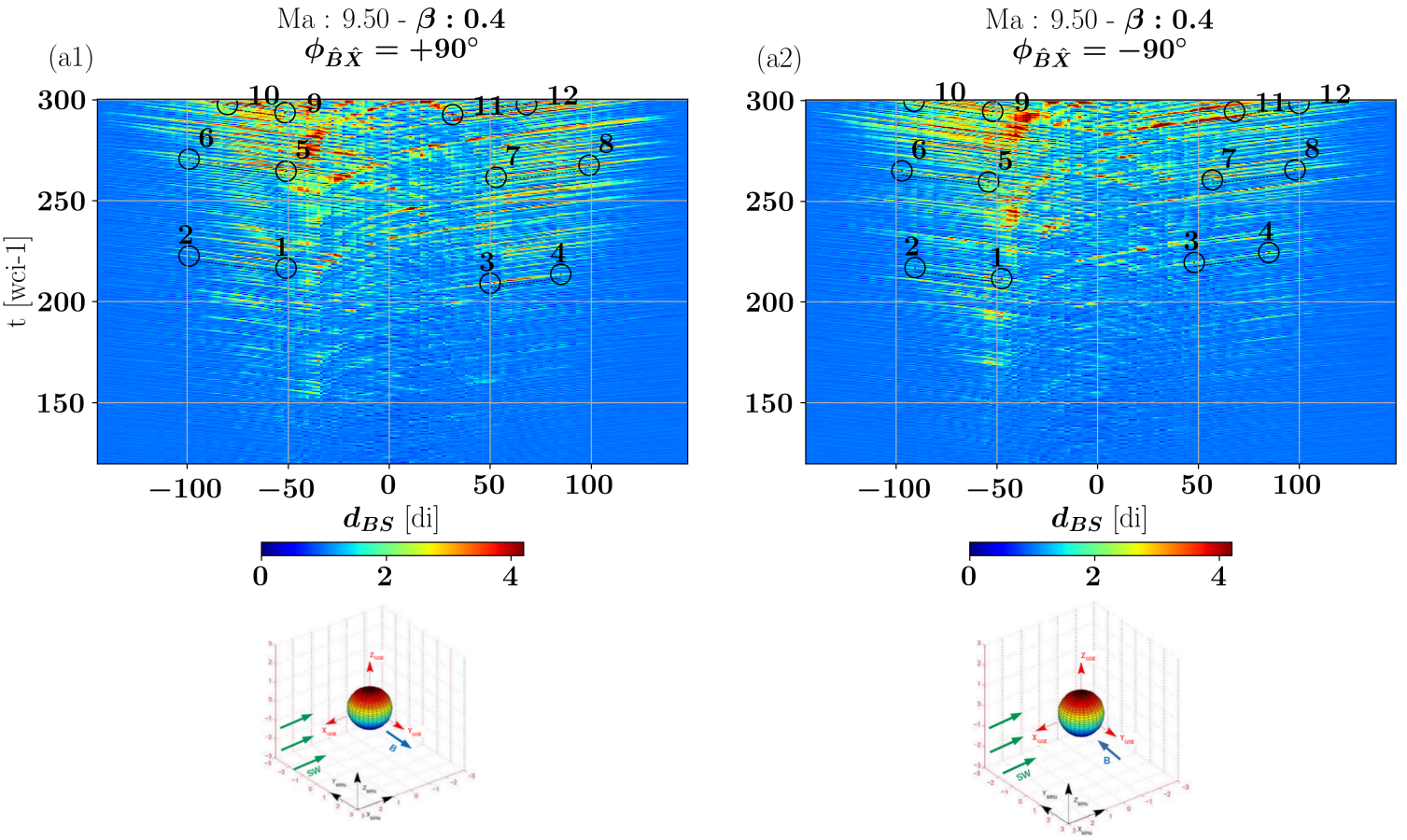

Fig. 4: Space-time plot of the Bow-Shock surface dynamics across the nominal surface for the cases with opposite IMF direction: Φ_{BX} represents the angle between the IMF direction and the X-coordinate in GSE coordinates. The X-axis represents the real distance between two points on the surface, in ion skin depths di, beginning from the Bow-Shock nose (d_{BS} = 0) towards the respective flank-ends. The numbered circles identify significant locations in the plot to compute the slope/ripples propagation velocity, summarized in Table II. Dashed black lines are used as reference for a better readability. Notice that the dotted lines have been slightly down-shifted for a better view of the propagating line.

Ma : 9.50 - $\beta = 0.4$ $\phi_{\hat{B}\hat{X}} = +90°$			Ma : 9.50 - $\beta = 0.4$ $\phi_{\hat{B}\hat{X}} = -90°$		
Points	Average Ripples Propagation Velocity [V_A]	Average Solar Wind Tangential Velocity [V_A]	Points	Average Ripples Propagation Velocity [V_A]	Average Solar Wind Tangential Velocity [V_A]
1-2	8.0	6.7	1-2	7.8	6.4
3-4	7.8	6.4	3-4	7.4	6.3
5-6	8.0	6.7	5-6	7.8	6.7
7-8	7.7	6.7	7-8	8.2	6.7
9-10	7.1	6.5	9-10	7.8	6.6
11-12	7.3	5.3	11-12	8.0	7.0
Average left wing (1-2, 5-6, 9-10)	**7.7**	**6.6**	**Average left wing (1-2, 5-6, 9-10)**	**7.8**	**6.6**
Average right wing (3-4, 7-8, 11-12)	**7.6**	**6.1**	**Average right wing (3-4, 7-8, 11-12)**	**7.9**	**6.7**
Total Average	**7.65**	**6.4**	**Total Average**	**7.8**	**6.6**

Table II: Ripples propagating velocities between the points marked in the space-time plots of the previous Figure, along with the average tangential velocity of the Solar Wind within the same paths.

From Figure 4 we can gain different insights:

(i) The locations of the ripples describe straight lines in time: these straight lines give the information that ripples propagate at approximately the same velocity along the surface. We can estimate this propagation velocity by estimating the slope in the plots for some meaningful locations, as marked by pair-points connected with dashed black lines in the plot and reported in Table II (values normalized to the Alfvén speed in the pristine conditions).
By using the nominal surface and considering that the Solar Wind bulk velocity flows mainly in the X-direction, we can estimate the local Solar Wind tangential velocity with respect to the plane under analysis (the out-of-plane component is neglected). The third column in Table II reports the corresponding average values for the respective pair of points.

(ii) Noticeably, in both the cases the propagation appears to predominantly begin at around |50| di from the BS nose, with the Dawn sector showing more intense signatures (e.g at -50 di), even in the case where the IMF is directed in the opposite direction.

(iii) The overall rippling dynamics however shows a more complicated pattern: we generally observe the formation of ripples distributions building up and lasting for some time around the same position (see e.g. the cluster in the area around d_{BS} ~ -50 di and t ~ 160 wci^{-1}), which indicates a steady ripples oscillation, followed later by a simultaneous linear propagation towards the flanks.

From the values in Table II, we can infer that the all ripples propagates at similar velocities (i.e. on average between 7 and 8 the value of the pristine Alfvén speed) independently of the side of the Bow-Shock, the evolution stage of the instability or, more importantly, of the IMF direction.

SECTION 4) CONCLUSIONS & ACKNOWLEDGEMENTS

We presented here some results from a set of hybrid simulations devoted to giving more insights into the tridimensional Bow-Shock response to different incoming Solar Wind Alfvénic Mach numbers at low-β and in a pure Quasi-Perpendicular interaction.

Particularly, we have found that:

- From a set of simulations, we observe an intense surface rippling clearly visible for Alfvénic Mach numbers as low as $M_A \sim 5$, yet these ripples were seen being smoothed out before achieving the flanks (results not shown here). Nevertheless, it is for relatively higher Mach numbers, such as $M_A = 9.5$ here studied, that we can appreciate an extended surface rippling propagating far down the Bow-Shock flanks.

- The rippling phenomenon occurs predominantly on the X-Y plane, whereas no rippling is observed on the perpendicular plane, which instead shows a very low frequency oscillation.

- By analyzing the space-time evolution of the BS surface:

  - The ripples are seen to propagate at a velocity nearly 7-8 times the pristine Alfvén speed in the cases analyzed here, independently of the upstream IMF direction. Also, ripples appear to propagate in line with the average tangential Solar Wind velocity within the same considered path.

  - The ripples are observed to hold the following pattern: they do not generate in the proximity of the BS nose, but yet several ion skin depths away. They firstly show a standing oscillating behavior, and later, oscillations propagate at a nearly constant velocity towards the Dusk region which can be observed also in the other direction.

Acknowledgements

The simulations were performed with the HPC resources available at CNRS / École Polytechnique, including the Zoidberg cluster and Hopper cluster.

The authors would like to thank Ronan Modolo for his support with LatHyS.

E.C. acknowledges the French National Research Agency, contract # ANR-17-CE31-0016-02.

M.A.T. acknowledges the French Innovation Agency AID, Convention 2778_IMES and the NASA 80NSSC20K1847 andNNN06AA01C funding.

After his experience at LPP, T.H. has recently started his PhD fellowship in the French Ærospace Lab at ONERA.

References

Jeřáb, M., et al. "Improved bow shock model with dependence on the IMF strength." Planetary and Space Science 53.1-3(2005): 85-93.

Burgess, D., and M. Scholer. "Shock front instability associated with reflected ions at the perpendicular shock." Physics ofPlasmas 14.1 (2007): 012108.

Turc, Lucile, et al. "3D hybrid simulations of the interaction of a magnetic cloud with a bow shock." Journal of GeophysicalResearch: Space Physics 120.8 (2015): 6133-6151.

Matthews, Alan P. "Current advance method and cyclic leapfrog for 2D multispecies hybrid plasma simulations." Journal ofComputational Physics 112.1 (1994): 102-116.

Modolo, Ronan, et al. "Influence of the solar EUV flux on the Martian plasma environment." Annales Geophysicæ. Vol. 23.
No. 2. Copernicus GmbH, 2005.

Johlander, Andreas, et al. "Rippled quasiperpendicular shock observed by the magnetospheric multiscale spacecraft."Physical review letters 117.16 (2016): 165101.

Hietala, H., and F. Plaschke. "On the generation of magnetosheath high-speed jets by bow shock ripples." Journal ofGeophysical Research: Space Physics 118.11 (2013): 7237-7245.

Winske, D., and K. B. Quest. "Magnetic field and density fluctuations at perpendicular supercritical collisionless shocks."Journal of Geophysical Research: Space Physics 93.A9 (1988): 9681-9693.